Two States of Cyclic Antimicrobial Peptide RTD-1 in Lipid Bilayers

Thomas M. Weiss,[‡] Lin Yang,[‡,§] Lai Ding,[‡] Alan J. Waring,[⊥,#] Robert I. Lehrer,[⊥] and Huey W. Huang*[,‡]

Department of Physics & Astronomy, Rice University, Houston, Texas 77251, and Departments of Medicine and Pediatrics, UCLA School of Medicine, Los Angeles, California 90095

Received March 22, 2002; Revised Manuscript Received May 28, 2002

ABSTRACT: RTD-1 is a recently discovered cyclic peptide that, like other well-studied antimicrobial peptides, appears to bind to the lipid matrix of cell membrane in the initial stage of activity. We studied the states of RTD-1 bound to lipid bilayers by two methods: oriented circular dichroism and X-ray diffraction. RTD-1 shows two physically distinct bound states in lipid bilayers like magainins, protegrins, alamethicin, and melittin that were previously studied. However, the nature of transition between the two states is different for RTD-1 as compared with the aforementioned peptides. In one of the two states, RTD-1 is oriented with its backbone ring parallel to the plane of the bilayer. Only in this state RTD-1 induces membrane thinning. But the effect of membrane thinning is much weaker than all other peptides, suggesting that the mechanism of RTD-1 may be different from the other peptides.

Vertebrate defensins arose from a common ancestral gene that existed before reptilian and avian lineages diverged. They are arginine-rich antimicrobial peptides with largely β-sheet structures that are stabilized by three intramolecular disulfide bonds. The two principal defensin subfamilies, alpha- and beta-defensins, differ in the placement and connectivity of their cysteine residues (*1, 2*). Recently, a third vertebrate defensin subfamily, called θ-defensins (or circular minidefensins) was discovered in granulocytes of the rhesus monkey (*Macaca mulatta*). The first described member of this subfamily was named RTD-1,[1] an abbreviation for rhesus theta defensin-1 (*3*). The θ-defensins are 18-residue cyclic peptides that are cross-linked by three disulfide bonds. This new molecular configuration differs from all other heretofore described antimicrobial peptides, which are mostly α-helical, β-sheet, or mixtures thereof (*4*−*7*).

So far, the experimental evidence indicates that θ-defensins behave like most other antimicrobial peptides, i.e., in the initial stage of their antibacterial activities they would bind to the lipid matrix, rather than protein receptors, in target cell membranes (*3*). In our previous studies on α-helical and β-sheet peptides, such as magainin (*8*−*10*) and protegrin (*11*−*13*), we found that peptides first bind to the membrane and embed themselves in the headgroup region of the lipid bilayer (the S state). Depending on the concentration of the peptides and the condition of the lipid bilayer, the peptides may remain in the S state or subsequently change into another state (the I state) wherein the peptides form transmembrane pores. Which of the two is the final state of a peptide at a given peptide concentration depends on the lipid composition of the bilayer and other factors that have not been fully investigated. Presumably, the propensity of a cell membrane to bind a peptide in its pore forming state (the I state) determines the susceptibility of the cell to the peptide. This propensity is determined by the stability of the S state relative to the I state. Thus, characterization of the bound states of a peptide to lipid bilayers is essential for understanding the mechanism of the peptide.

It is far from certain that the molecular mechanism of θ-defensins will follow the same pattern as magainin and protegrin. While most known antimicrobial peptides exhibit an amphiphilic character in their membrane-bound molecular configurations, a recent NMR study reported that the structure of RTD-1 lacks the amphiphilic character but has a significant flexibility (*14*). In a somewhat related study on peptide−membrane interactions, a 16-residue peptide, called penetratin, exhibits a change of structure from α-helix to β-sheet as a function of the peptide−lipid ratio (*15*). Such richness and versatility of peptide-membrane interactions prompted us to study this novel cyclic peptide RTD-1.

In this paper, we report our experimental results with RTD-1 using the methods of oriented circular dichroism (OCD) (*16*, *17*) and X-ray lamellar diffraction (*18*). Like all other peptides we have investigated, RTD-1 exhibited two distinct states of binding to lipid bilayers. However, the nature of the transition between these two states is quite different from other peptides. One of the two states has an OCD spectrum of β-sheets with light incident normal to the plane of the sheets (*19*). X-ray lamellar diffraction showed that RTD-1 in this state induces membrane thinning (*20*) in

[†] H.W.H. was supported by NIH Grant GM55203 and by the Robert A. Welch Foundation; R.I.L. was supported by NIH Grants AI-22839 and AI37945.

* To whom correspondence should be addressed: Department of Physics & Astronomy, Rice University, Houston, TX 77251-1892. Telephone: (713)348−4899. Fax: (713)348−4150. E-mail: hwhuang@rice.edu.

[‡] Rice University.

[⊥] Department of Medicine, UCLA School of Medicine.

[#] Department of Pediatrics, UCLA School of Medicine.

[§] Current address: National Synchrotron Light Source, Brookhaven National Laboratory, Upton, NY 11973.

[1] Abbreviations: RTD-1, cyclic (GFCRC LCRRG VCRCI CTR); PG-1, protegrin-1; DLPC, 1,2-dilauroyl-*sn*-glycero-3-phosphocholine; DMPC, 1,2-dimyristoyl-*sn*-glycero-3-phosphocholine; DMPG, 1,2-dimyristoyl-*sn*-glycero-3-[phospho-rac-(1-glycerol)] (sodium salt); POPC, 1-palmitoyl-2-oleoyl-*sn*-glycero-3-phosphocholine; OCD, oriented circular dichroism; RH, relative humidity; P/L, peptide-to-lipid molar ratio.

10.1021/bi025853d CCC: $22.00
Published on Web 07/09/2002

proportion to the peptide-to-lipid ratio. Thus, we were able to identify this state as the S state. In the other state, RTD-1 did not thin the membrane. Whether the peptide induces transmembrane pores in this state will be investigated in future experiments using neutron and synchrotron radiation facilities. Here we show the similarities and differences between RTD-1 and the other antimicrobial peptides.

MATERIALS AND METHODS

Sample Preparation. RTD-1 (GFCRC LCRRG VCRCI CTR) was synthesized as described in ref *21*. Briefly, RTD-1 was synthesized by FastMoc chemistry on a Perkin-Elmer ABI 433 A Peptide synthesizer at a 0.25-mmol scale. We used prederivatized poly(ethylene glycol) polystyrene arginine resin (PerSeptive Biosystems, Framingham, MA) and double coupled all residues for optimal yield. The crude synthetic peptide was reduced under nitrogen for 15 h at 50 °C, using excess dithiothreitol in 6 M guanidine·HCl, 0.2 M Tris·HCl, and 0.2 mM EDTA (pH 8.2). This reaction was terminated by adding glacial acetic acid to a 5% final concentration. The reduced peptide was stored under nitrogen until purified to virtual homogeneity by RP-HPLC. The disulfide bonds were formed by dissolving the reduced peptide at 0.1 mg of peptide/mL in 0.1% acetic acid. Ammonium hydroxide was added to adjust the pH to 7.4, and the solution was stirred for 24 h at room temperature before adding acetic acid (5% final concentration) to stop the reaction. To form an amide bond linking the amino and carboxy-termini, the oxidized peptide was incubated for 18 h at room temperature in a 3:1 mixture of ethylenediaminecarbodiimide and anhydrous *N*-hydroxybenzotriazole in dimethyl sulfoxide. The cyclized product was lyophilized and purified by reverse phase-HPLC on a C18 column with a linear gradient of acetonitrile/water in 0.1% trifluoroacetic acid. All steps were monitored by MALDI-MS and analytical RP-HPLC.

1,2-Dilauroyl-*sn*-glycero-3-phosphocholine (DLPC), 1,2-dimyristoyl-*sn*-glycero-3-phosphocholine (DMPC), 1,2-dimyristoyl-*sn*-glycero-3-[phospho-rac-(1-glycerol)] (sodium salt) (DMPG), and 1-palmitoyl-2-oleoyl-*sn*-glycero-3-phosphocholine (POPC) were purchased from Avanti Polar Lipids (Alabaster, AL). Chloroform and trifluroethanol (TFE) were purchased from Sigma Chemicals Co. (St. Louis, MO). All chemicals were used without further purification.

Sample preparations for both the CD and X-ray measurements followed the method described in Ludtke et al. (*9*) and Heller et al. (*11*). For solution CD with lipid vesicles, the peptide and lipids at a chosen molar ratio, P/L, were mixed in organic solvent. The solvent was blown off under dry N_2 and removed under vacuum. Distilled water was added to the mixture to result in a total vesicle concentration of 1 mg/mL, which was then vortexed vigorously and sonicated for a period of 10 min before the measurement. For oriented circular dichroism (OCD) and X-ray lamellar diffraction, oriented multilayered samples were used. First, solid substrates, quartz plates for OCD and polished silicon wafers for X-ray, were cleaned in hot sulfuric−chromic acid and rinsed thoroughly first with distilled water and then with ethanol. The plates were dried in an oven, ready for use. Next, a total amount of 0.3−0.5 mg of lipid was codissolved with peptide at the desired P/L in a mixture of chloroform and TFE. The dissolved mixture was deposited on a cleaned substrate, and the solvent was allowed to evaporate. During the evaporation of the solvent, the sample self-assembled into aligned multilayers parallel to the substrate surface. The chloroform/TFE ratio was varied ranging from 3:1 to 1:3 (vol/vol) to optimize the uniformity of the sample on the substrate (*9*). Once the solvent evaporated, it was placed in a vacuum freeze-dryer for at least 1 h to ensure a complete removal of the solvent residues. The vacuumed sample was then slowly hydrated in a temperature−humidity chamber. A good sample had a visually smooth and flat surface, and showed six to eight orders of Bragg diffraction peaks by X-ray, indicating that it was a stack of parallel lipid bilayers. The degree of alignment was measured by a two-dimensional ω vs 2θ scan (see below).

Temperature−Humidity Control. For both OCD and X-ray experiments, the sample was housed in a temperature−humidity chamber. The X-ray chamber consisted of a base mounted on a standard goniometer head and a cover that fits tightly onto the base. The cover was made of aluminum with Beryllium windows for the passage of X-rays. It was temperature controlled using two thermoelectric modules (Melcor Electronics Corp., Trenton, NJ) driven by an electronic feedback circuit. During measurement, the cover was kept ∼5 °C above the sample temperature to prevent condensation of water on the walls and windows of the chamber when measuring at high humidities. The chamber base contained a temperature controlled aluminum plate onto which the sample was mounted and through which the sample temperature could be controlled. The humidity inside the chamber was regulated by heating or cooling a small water bath inside. The controls for the temperature of the sample mount and the relative humidity of the air surrounding it were feedback circuits that responded to the outputs of the temperature and humidity probes. The feedback circuits provided heating or cooling using thermoelectric modules. The temperature probe was an AD590 two-terminal IC temperature transducer, calibrated at 0 °C with a mixture of ice and water and at 35 °C with a calibrated Fisher digital thermometer. The relative humidity probe was an EMD-2000 (General Eastern Instruments, Woburn, MA). The RH was calculated based on the impedance−RH table provided with the probe. Both probes were placed onto the sample mount in the immediate vicinity of the sample. With this chamber, we were able to change the temperature and humidity to a set value within minutes. The temperature could be controlled to within ± 0.05 °C. The relative humidity in the vicinity of sample could be controlled to within ± 0.5% RH in most cases.

The chamber for the OCD experiment was made similarly, but using quartz plates as windows for the passage of UV light. Water condensation on the windows was prevented by heating the whole sample compartment of the spectropolarimeter above the sample temperature.

Oriented Circular Dichroism. Oriented circular dichroism is a simple method for detecting the orientation change of peptides embedded in lipid bilayers using a conventional CD machine (*16*, *17*). A Jasco J-500A spectropolarimeter was used for this experiment. The procedure of OCD measurement is the same as the conventional CD measurement, except that an oriented sample is used. For most experiments as in this one, normal (rather than oblique) incidence OCD

is sufficient for spectral analysis (*17*). The sample mount for OCD was allowed to rotate around an axis normal to the surface of the sample substrate and coincident with the incident light. We made sure that OCD did not change with the rotational angle (*17*).

X-ray Lamellar Diffraction. The sample mount for lamellar diffraction was allowed to rotate (angle ω) around an axis normal to the plane of scattering. Lamellar diffraction was collected on an Enraf Nonius Diffractus 581 and a Huber four-circle goniometer, with a line-focused (10 mm vertical $\times$ 1 mm horizontal) Cu Kα source ($\lambda = 1.542$ Å) operating at 40 kV and 15−30 mA. At a 6° takeoff angle (the projected source dimension 10 $\times$ 0.1 mm^2), the incident beam was collimated by a horizontal soller slit and two vertical slits on the front and the backsides of the soller slit. The horizontal and vertical divergence of the incident beam were 0.23° and 0.3°, respectively. The diffracted beam first passed through a vertical slit and then was discriminated by a bent graphite monochromator before entering a scintillation detector which was biased to discriminate against higher harmonics. A diffracted beam monochromator has the advantage over an incident beam monochromator in that the Compton scattering and the fluorescence from the sample are screened; consequently, the background signal is greatly reduced, that in turn allows the measurement of high diffraction orders.

One unique feature of membrane diffraction is that the repeat spacing is more than 30 times the X-ray wavelength. The momenta **q** satisfying the Bragg law lie very close to the surface of the Ewald sphere. As a consequence, it is very easy to obtain incorrect diffraction amplitudes with the sample misaligned in χ without realizing it. (χ is the rotational angle around the line of intersection between the plane of scattering and the sample plane.) We have established an elaborate routine for positioning and orienting lamellar samples, which was described in Wu et al. (*20*). A two-dimensional $\omega-\theta$ scan around the second or third Bragg order was used to check the alignment of the ω-angle (see Figure 5 below). A correctly aligned sample has the peak position exactly at $2\omega = 2\theta$ in the $\omega - \theta$ plane. Also, the quality of the sample could be assessed from this scan: a well-aligned sample exhibited a single Bragg peak on a flat even background, whereas poor alignment showed up as a broad shoulder along ω. Samples where the shoulder amounted to more than 5% of the peak intensity were rejected.

Diffraction patterns of good samples were recorded by $\omega-2\theta$ scan, repeated four to five times every hour from $\omega = 0°$ to 10° with the step size $\Delta\omega = 0.02°$. An Al-attenuator was used to reduce the count rate for the first two diffraction orders in order not to saturate the detector. The data were taken at 35 °C for the DMPC samples (at 25 °C for the DLPC samples to ensure that the bilayers were in the fluid phase at high humidities), for a series of humidity settings ranging from RH 70% to 99%. Only consecutive scans that overlapped within the experimental error indicating that the sample conditions did not change during the scan were averaged and subsequently analyzed. For each sample, data sets consisting of scans for 5−10 different relative humidities at the same temperature were collected. Also, several samples of the same lipid−peptide composition were measured to ensure reproducibility.

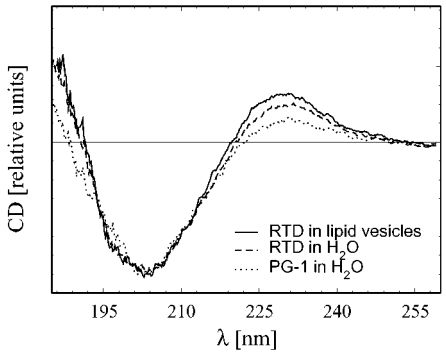

FIGURE 1: Solution circular dichroism (CD) of RTD-1 in water in the absence (dashed line) and presence (solid line) of lipid vesicles (DMPC/PG 1:1, molar) at a peptide-to-lipid molar ratio of 1:30. The secondary structure of the peptide did not change by its association with the lipid bilayers. For comparison, the solution CD of protegrin PG-1 in water (dotted line) is also shown. Both peptides have β-sheet secondary structures.

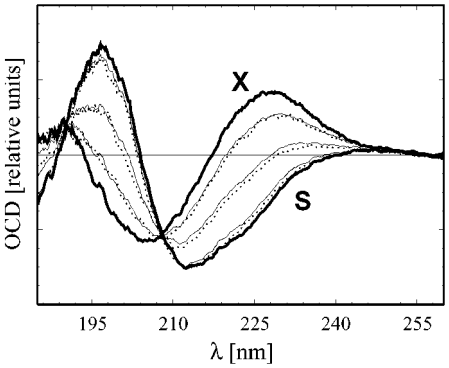

FIGURE 2: Oriented circular dichroism (OCD) of RTD-1 in DMPC/PG (1:1) bilayers, depicting the spectra of the two binding states, X and S, of RTD-1 together with a few intermediates. The spectra were obtained by raising the hydration of the sample with the relative humidity RH changing from 90 to 99%. The sample initially displayed spectrum X, gradually changed over to spectrum S, through the intermediate states. Upon decreasing the humidity from 99 to 90%, the spectrum reversed from S to X. (X and S in thick solid lines and three intermediate states in dotted lines are data. The thin solid lines are fits to the intermediate states with a linear combination of S and X.)

RESULTS

Solution Circular Dichroism. Figure 1 shows the CD spectra of RTD-1 in an aqueous solution and in a DMPC/PG (3:1) vesicle solution. Like most other antimicrobial peptides, RTD-1 is a cationic peptide. (RTD-1 carries +5 charges as compared to +6 for protegrin PG-1, +6/-1 for magainin, and +6 for melittin.) It has been demonstrated that in the presence of negatively charged lipid vesicles, such as DMPC/PG, cationic peptides are bound to lipid bilayers (*22*). However, since RTD-1 has a stable cyclic structure with three intramolecular disulfide bonds, it is as expected that the CD of the peptide undergoes no changes upon binding to lipid vesicles. This is contrary to, for example, magainins that, in a similar experiment, would change from a random coil in a water solution to a helical configuration upon adding lipid vesicles (*22*). The closeness of the two CD spectra for RTD-1 and protegrin PG-1 (*11*) is not surprising either, since both peptides have β-sheet secondary structures (*3*).

Oriented Circular Dichroism. Figure 2 shows a series of OCD spectra of RTD-1 bound to DMPC/PG (1:1) bilayers

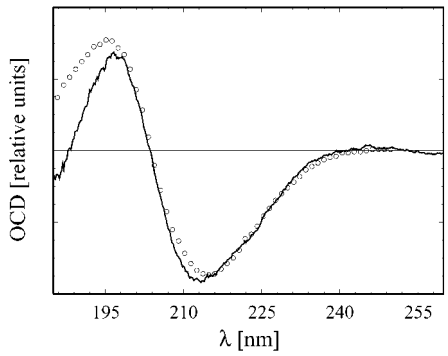

FIGURE 3: OCD spectrum of the S state of RTD-1 (solid line) compared with the spectrum of an oriented β-sheet polypeptide, poly(Leu−Lys) as measured by Bazzi and Woody (*19*) (circles). The similarity of the two spectra suggests that the backbone ring of the RTD peptide is parallel to the plane of the membrane. The photon counts below 195 nm are typically low in CD measurements due to strong UV absorption. Thus, the discrepancy in this region may be insignificant.

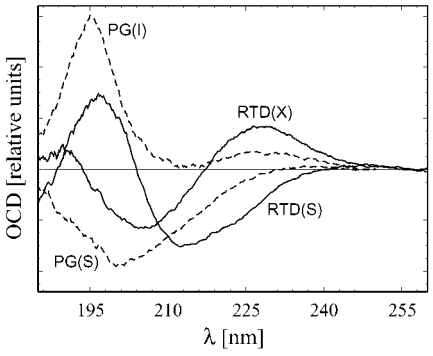

FIGURE 4: The OCD basis spectra of RTD-1, RTD(X), and RTD-(S), compared with the OCD basis spectra of PG-1, PG(I), and PG(S) [from Heller et al. (*11*)]. Both peptides exhibit two distinct states of binding to lipid bilayers. Despite their similar solution CD spectra, their OCD spectra for the two states are rather different. (The two basis spectra of each peptide are normalized to each other, but the absolute magnitudes are not normalized.)

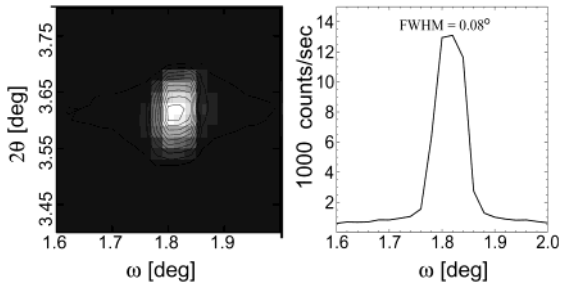

FIGURE 5: A representative two-dimensional $\omega-\theta$ scan around the 2nd order Bragg peak of an aligned multilayer sample of RTD-1 in DMPC at P/L = 1/10 (left). The sample was prepared in state S. The sample was well aligned and showed a single peak on a flat background. A cut through the center of the peak at constant 2θ corresponds to the ω rocking curve, which exhibits a fwhm of 0.08°.

at P/L = 1/30. The spectra were measured at 35 °C (the same as the X-ray experiment) and the relative humidity (RH) was increased in steps of 2.5%. The sample exhibited the spectrum named X for RH values up to 90%. Then, the spectrum started to change gradually toward the spectrum named S, which was reached near full hydration. All intermediate states can be fit with linear combinations of the S and X spectra, indicating that they are mixtures of the S state and the X state. This transition could be reversed by lowering the RH from high to low values, indicating that the peptide was undergoing a physical change of orientation rather than a chemical alteration. Samples with different peptide-to-lipid ratios were measured where a weak concentration dependence was observed. Increasing the peptide concentration shifted the transition to higher RH values and also shortened the RH range over which the transition was taking place. Lowering the concentration below P/L = 1/30 on the other hand led to a stabilization of the S state to the extent that the transition stopped being reversible. We also varied the relative content of DMPC versus DMPG ranging from PC/PG = 1/3 to PC/PG = 3/1. We observed that increasing the ratio of PC lipids in the sample also had a stabilizing effect on the S state, so that at a ratio of PC/PG > 1:1 the transition from X to S was irreversible. We have experimented with a variety of lipid compositions, including DMPC/PG mixtures, DLPC, and POPC. The general behavior of RTD-1 is that in the initial low-hydration conditions the peptide is in the X state. Upon reaching high-hydration conditions, the peptide changes to the S state. In the absence of negatively charged lipids, the X → S transition seems to be irreversible.

Figure 3 shows the comparison of the S spectrum with an OCD of the β-sheet polypeptide, poly(Leu−Lys), that was independently measured by Bazzi and Woody (*19*). The polypeptides were deposited on a substrate and the CD of poly(Leu−Lys) was measured with light incident normal to the substrate surface. The essential agreement between the S spectrum and the CD of oriented poly(Leu−Lys) implies that in the S state the ring of the RTD backbone is parallel to the plane of the bilayer.

Figure 4 compares the OCD spectra of RTD-1 with that of protegrin PG-1 (*11*). Since both peptides are β-sheets and have nearly the same solution CD (Figure 1), the differences between RTD-1 and PG-1 indicate that the orientations of their bound states are different. In the case of α-helical peptides, the optical activity tensor has one principal axis parallel to the helical axis and two degenerate principal axes perpendicular to the helical axis (*23*). The two OCD spectra, one parallel to the helical axis and one perpendicular to the helical axis, are sufficient for the reconstruction of the orientationally averaged vesicle CD (*17*). In the case of β-sheet peptides, the optical activity tensor has three distinct principal axes. Therefore, it is impossible to reconstruct the vesicle CD (Figure 1) from the two OCD spectra, X and S.

X-ray Diffraction. The quality of a multilayer sample was examined by a two-dimensional $\omega-\theta$ scan around the second or third Bragg order (Figure 5, left). A correctly aligned sample has the peak position exactly at $2\omega = 2\theta$. The conventional rocking curve was obtained by a cut at constant 2θ through the peak (Figure 5, right). The width of the peak (∼0.08°) is the same as the limiting resolution of our apparatus, implying extremely good alignment of the multilayers, even at a peptide concentration as high as P/L = 1/10. Typical diffraction patterns from pure DMPC and DMPC with high concentrations of RTD-1 are shown in Figure 6. In general, the higher the peptide concentration, the harder it is to achieve high orders of diffraction due to the propensity for poor sample quality. However, by careful preparation of the multilayer samples, we were able to obtain the same number of diffraction orders for high peptide

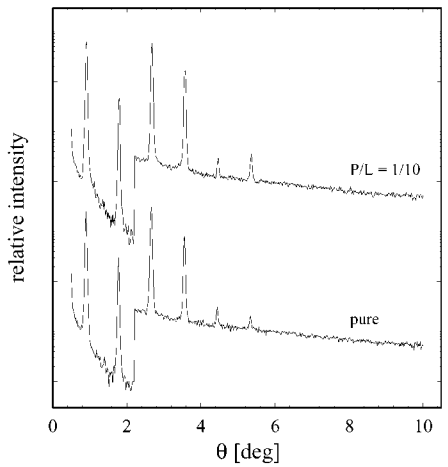

FIGURE 6: Representative diffraction patterns of pure DMPC (bottom) and DMPC with RTD-1 at P/L = 1/10 (top) at an intermediate RH value (repeat spacing ~51 Å). All samples measured showed at least six discernible Bragg peaks up to high hydration levels. The patterns are vertically displaced for clarity. The step between the second and the third peak was due an X-ray attenuator that was used for the first two peaks to avoid detector saturation.

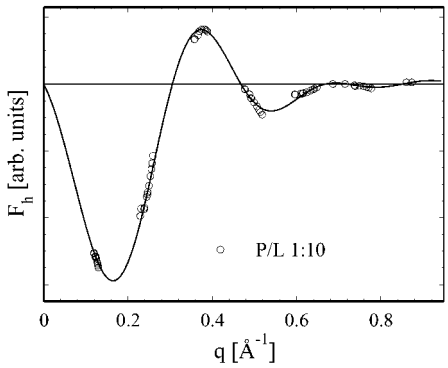

FIGURE 7: Representative phasing diagram for RTD-1 in DMPC at P/L = 1/10. The corrected and scaled amplitudes can be connected by a smooth curve, showing the correct assignment of the phases. The solid curve was constructed by using one set of diffraction amplitudes (*18*).

concentrations as for a pure lipid. The data reduction procedure has been described in detail in previous publications (*18*, *20*, *24*). Briefly, it consists of the following steps. A background curve was generated by removing all of the Bragg peaks from all of the data sets of a particular sample, and then averaging the results and interpolating over any remaining gaps. After the background removal, a correction for the sample size vs the beam size, i.e., the diffraction volume, together with the absorption correction was carried out for each data point. Each Bragg peak was then fit with a Gaussian and integrated to obtain the intensity of that order. The integrated intensity was corrected for the polarization and the Lorentz factors. The square root of the integrated intensity is the relative magnitude of the scattering amplitude. The phase problem was solved by the swelling method (*18*). Figure 7 shows an example of the highest peptide concentration P/L = 1/10. The diffraction amplitudes of 11 different degrees of hydration all fall on a smooth curve by a correct assignment of the phases. With the phases determined, the relative scattering amplitudes were Fourier transformed to produce unnormalized electron density profiles (Figure 8), from which the peak-to-peak (PtP) distance was measured.

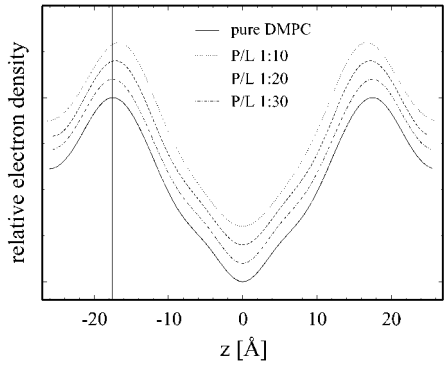

FIGURE 8: Electron density profiles for pure DMPC and DMPC/RTD bilayers. The repeat spacings for the profiles shown were ~51 Å. The profiles are shifted vertically for clarity. The vertical line shows the peak position of the pure DMPC profile.

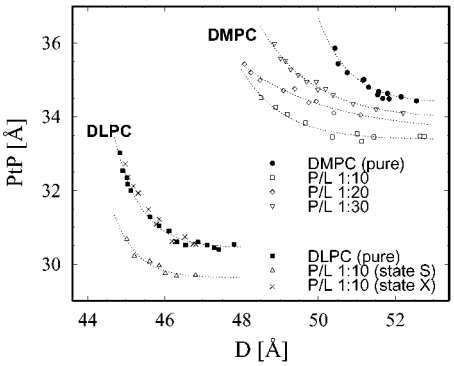

FIGURE 9: The peak-to-peak distance (PtP) of DMPC and DLPC bilayers with and without peptide as a function of the repeat spacing D. Since the repeat spacing is a measure for the hydration of the bilayer, one can extract the bilayer thickness at full hydration by extrapolation. The lines in the figure represent an exponential fit to the data points ($a_o + e^{-(x-x_o)/a_1}$), intended as guides for the extrapolation. RTD-1 in the DMPC bilayers was monitored by OCD to be in the S state. The thickness of the DMPC bilayer was reduced in the presence of RTD-1, in proportion to P/L (see Figure 10). In the case of DLPC with RTD (P/L = 1/10), the RTD-1 was initially in the X state during the first series of scan (cross symbols). RTD-1 was subsequently in the S state during the second series of scan (triangular symbols). While the state S thinned the membrane, the state X did not affect the bilayer thickness.

PtP is unaffected by normalization of the electron density profile (*20*). Figure 9 shows the PtP of DMPC with and without RTD-1 (in the state S) at various peptide-to-lipid ratios, P/L, plotted as a function of the repeat spacing D. The membrane thickness at full hydration can be extracted from such plots by extrapolating the PtP to high repeat spacings. To that end, an exponential decay (plus a constant) was fit to the data as shown in Figure 9. The result is shown in Figure 10, where the PtP at full hydration is plotted as a function of the peptide-to-lipid ratio P/L.

Figure 9 also shows PtP measurements of pure DLPC and DLPC with RTD-1 at P/L = 1/10. OCD measurements indicated that the RTD-1 was initially in the X state during the first series of scans. RTD-1 was subsequently in the S state during the second series of scans. While the state S thinned the membrane, the state X did not affect the bilayer thickness.

DISCUSSION

The most important result of our experiment is that RTD-1 shows two physically distinct bound states in lipid bilayers.

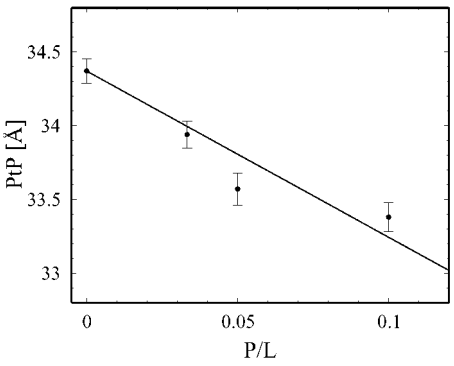

FIGURE 10: The PtP at full hydration of DMPC bilayers as a function of the P/L as extracted from Figure 9. The error bars represent the RMS deviation from the exponential fit to the data points. The straight line represents a fit to the data points. Compared with other antimicrobial peptides the thinning effect of RTD-1 is rather weak.

RTD-1 was incorporated into bilayers of various lipid compositions at a variety of peptide−lipid ratios. For experimental convenience, we changed the temperature and the hydration condition of the bilayers to vary their physical properties so as to explore the binding state of RTD-1 in a variety of bilayer conditions. In particular, we know that hydration changes can significantly alter the membrane's elastic properties and thickness (*20*, *25*). Thus, in such an experiment, the peptide has been tested in lipid bilayers over a wide range of thermodynamic conditions. In all cases, its OCD was either one of the two extreme spectra S or X, or a linear combination of the two. Thus, the cyclic peptide RTD-1 conforms to the two-state model that was previously deduced from extensive studies of magainin, protegrin, alamethicin, melittin, and their analogues (*13*). To date, it seems that all antimicrobial peptides, irrespective of their secondary structures, exhibit two distinct states of binding to lipid bilayers.

An important reference for the OCD spectra of RTD-1 is the CD spectrum of oriented β-sheet polypeptide, poly(Leu−Lys), that was independently measured by Bazzi and Woody (*19*) as shown in Figure 3. The polypeptides were deposited on a substrate by the isopotential spin-dry method. Polarized infrared measurements showed that the plane of the β-sheets was parallel to the plane of the substrate within an uncertainty of 14°. This OCD of poly(Leu−Lys) was measured with light incident normal to the substrate surface, and is essentially the same as the S state OCD of RTD-1. (The quantitative discrepancy below 195 nm may be insignificant, because CD in this region often contains large uncertainties due to strong UV absorption). According to the geometry of our OCD measurement, this implies that the ring of the RTD backbone is approximately parallel to the plane of the bilayer. This molecular orientation and the membrane thinning effect observed in the S state (but not in the X state) seem to imply that RTD-1 in the S state is embedded in the headgroup region. However, the S state of RTD-1 is rather different from the S state of other antimicrobial peptides.

Although the S state RTD-1 induces a membrane thinning effect similar to those caused by other peptides (*9*, *12*, *20*), the effect is only approximately one-tenth as strong. Both alamethicin (*20*) and magainin (*9*) induced a membrane thinning of about 2 Å at P/L $\sim$ 1/50, and protegrin (*12*) about 1 Å at P/L $\sim$ 1/70. From the area per lipid, we deduced that such thinnings correspond to an expansion of the membrane area per peptide from 200 to 350 Å^2 that are approximately the cross sections of these peptides along their long axes. Therefore, we concluded that alamethicin, magainin, and protegrin in their S state are fully embedded in the headgroup region of the lipid bilayer with their long axes oriented parallel to the bilayer. In comparison, RTD-1 induced a membrane thinning of about 1 Å at P/L $\sim$ 1/10. If we follow the same line of deduction, it would imply that RTD-1 in the S state is only partially embedded in the headgroup region. In fact, this is consistent with the relatively weak concentration dependence of RTD-1 as observed in the OCD experiment. For the other peptides, whenever there is a hydration-dependent S−I transition (*26*, *27*), there is also a strong dependence on the peptide concentration P/L. This was explained as due to the energy cost of membrane thinning (*28*, *29*), i.e., the elastic energy of thinning increases the energy level of the S state by a term proportional to $(P/L)^2$ that causes the transition to the I state as P/L increases. In the case of RTD-1, both its membrane thinning effect and its concentration dependence are very weak in comparison.

There are other differences between RTD-1 and the other peptides. In previous studies on oriented multilayer membranes (*30*, *31*), we have demonstrated that at full hydration the individual membranes are uncorrelated and their properties approach that of a freely undulating membrane. Thus, fully hydrated membranes are considered to be close to the physiological conditions. For all other membrane-active peptides we have investigated, both of their I state and S states were found in fully hydrated lipid bilayers if a variety of lipid compositions were tried. But so far the X state of RTD-1 has not been found in any fully hydrated lipid bilayer. In particular, all other peptides bound to fully hydrated DMPC bilayers were found to be in the I state (in the observable range of P/L $>$ 1/200). This was explained as due to the fact that DMPC has a high headgroup-to-chains area ratio compared with lipids of unsaturated chains, thus less favorable for the peptides to adsorb in the headgroup region (*27*, *29*). So far, RTD-1 is the only exception in that it binds to fully hydrated DMPC bilayers in the S state in a P/L ratio as high as 1/10. As mentioned above, dehydration alters the bilayer properties, and so far the X state of RTD-1 has only been found in less than fully hydrated states. Therefore, although the X state exists and is characterized by a well-defined OCD, whether it has a physiological correspondence is uncertain.

Thus, although RTD-1 exhibits two binding states to lipid bilayers like other antimicrobial peptides, we do not know if it utilizes the same molecular mechanism as others in its activities. Recently, RTD-1 and related primate circular minidefensins were shown to protect CD4-positive human cells from in vitro infection by HIV-1 (AIDS) retroviruses (*32*). Additionally, these peptides show a distinct lack of cytotoxicity, even though confocal fluorescent microscopy revealed the formation of patch-like peptide aggregates on the cell surface (*32*). Further investigation on the similarities and differences between RTD-1 and other peptides may shed light on the functions of antimicrobial peptides in general and on those of circular (θ) minidefensins in particular.

REFERENCES

1. Liu, L., Zhao, C., Heng, H. H., and Ganz, T. (1997) *Genomics 43*, 316−320.
2. Zhao, C., Nguyen, T., Liu, L., Sacco, R. E., Brogden, K. A., and Lehrer, R. I.. (2001) *Infect. Immun. 69*, 2684−2691.
3. Tang, Y. Q., Yuan, J., Osapay, G., Osapay, K., Tran, D., Miller, C. J., Ouellette, A. J., and Selsted, M. E. (1999) *Science 286*, 498−502.
4. Boman, H. G., Marsh, J., Goode., J. A., Eds. (1994) *Antimicrobial Peptides*, pp 1−272, Ciba Foundation Symposium 186, John Wiley & Sons, Chichester.
5. Martin, E., Ganz, T., and Lehrer, R. I. (1995) *J. Leukocyte Biol. 58*, 128−136.
6. Hoffmann, J. A., Kafatos, F. C., Janeway, C. A., and Ezekowitz, R. A. B. (1999) *Science 284*, 1313−1318.
7. Ganz, T. (1999) *Science 286*, 420−421.
8. Ludtke, S. J., He, K., Wu, Y., and Huang, H. W. (1994) *Biochim. Biophys. Acta 1190*, 181−184.
9. Ludtke, S., He, K., and Huang, H. W. (1995) *Biochemistry 34*, 16764−16769.
10. Ludtke, S. J., He, K., Heller, w. T., Harroun, T. A., Yang, L., and Huang, H. W. (1996) *Biochemistry 35*, 13723−13728.
11. Heller W. T., Waring, A. J., Lehrer, R. I., and Huang, H. W. (1998) *Biochemistry 37*, 17331−17338.
12. Heller W. T., Waring, A. J., Lehrer, R. I., Harroun, T. A., Weiss, T. M. Yang, L., Huang. H. W. (2000) *Biochemistry 39*, 139−145.
13. Huang, H. W. (2000) *Biochemistry 39*, 8347−8352.
14. Trabi, M., Schirra, H. J., and Craik, D. J. (2001) *Biochemistry 40*, 4211−4221.
15. Magzoub, M., Eriksson, L. E. G., and Graslund, A. (2002) *Biochemistry*, to be published.
16. Olah, G. A., and Huang, H. W. (1988) *J. Chem. Phys. 89*, 2531−2538.
17. Wu, Y., Huang, H. W., and Olah, G. A.. (1990) *Biophys. J. 57*, 797−806.
18. Olah, G. A., Huang, H. W., Liu, W., and Wu, Y. (1991) *J. Mol. Biol. 218*, 847−858.
19. Bazzi, M., and Woody, R. W. (1987) *Biopolymers 26*, 1115−1124.
20. Wu, Y, He, K., Ludtke, S. J., and Huang, H. W. (1995) *Biophys. J. 68*, 2361−2369.
21. Leonova, L., Kokryakov, V. N., Aleshina, G., Hong, T., Nguyen, T., Zhao, C., Waring, A. J., and Lehrer, R. I. (2001) *J. Leukoc. Biol. 70*, 461−464.
22. Matsuzaki, K., Harada, M., Handa, T., Funakoshi, S., Fujii, N., Yajima, H., and Miyajima, K. (1989) *Biochim. Biophys. Acta 981*, 130−134.
23. Tinoco, I., and Hammerle, W. G. (1956) *J. Phys. Chem. 60*, 1619−1623.
24. Chen, F. Y., Hung, W. C., and Huang, H. W. (1997) *Phys. Rev. Lett. 79*, 4026−4029.
25. Chen, S. H., Liao, C. Y., Huang, H. W., Weiss, T. M., Bellisent-funnel, M. C., and Sette, F. (2001) *Phys. Rev. Lett. 86*, 740−743.
26. Huang, H. W., and Wu. Y. (1991) *Biophys. J. 60*, 1079−1087.
27. Heller, W. T., He, K., Ludtke, S. J., Harroun, T. A., and Huang, H. W. (1997) *Biophys. J. 73*, 239−244.
28. Huang, H. W. (1995) *J. Phys. II France 5*, 1427−1431.
29. Chen, F.-Y., Lee, M.-T., and Huang, H. W. (2002) *Biophys. J. 82*, 908−914.
30. Yang, L., Weiss, T. M., Harroun, T. A., Heller, W. T., and Huang, H. W. (1999) *Biophys. J. 77*, 2648−2656.
31. Yang, L., Weiss, T. M., Lehrer, R. I., and Huang, H. W. (2000) *Biophys. J. 79*, 2002−2009.
32. Cole, A. M., Hong, T., Boo, L. M., Nguyen, T., Zhao, C., Bristol, G., Zack, J. A., Waring, A. J., Yang, O. O., and Lehrer, R. I. (2002) *Proc. Natl. Acad. Sci. U.S.A. 99*, 1813−1818.

BI025853D